A vibrating fiber microbalance for measuring layer-by-layer adsorption on graphite

L. Bruschi and G. Torzo
Dipartimento di Fisica G. Galilei-Università di Padova, via Marzolo 8, 35131 Padova, Italy

(Received 2 May 1991; accepted for publication 8 July 1991)

This article describes an improved version of the graphite fiber microbalance, a device that was recently proved to be a useful tool for investigating adsorption phenomena. Hydrodynamic effects, that may yield large errors in the calculation of the adsorbed mass, if not properly evaluated, are carefully accounted for. An accurate measurement of the film coverage is obtained by using a correction to Stokes equations in the region of semiballistic regime that is much simpler than the slip theory used by other authors.

I. INTRODUCTION

The graphite fiber microbalance is a recent technique that has been used to investigate the growth behavior of films physisorbed onto graphite.[1–4] The informations given by this technique, both in the submonolayer and in the thick-film regime, are complementary to those offered by ellipsometry, by electron and neutron diffraction, and by volumetric adsorption isotherms.[5] The microbalance measures the *total* adsorbed mass, while ellipsometric technique only monitors the *last adsorbed layer*. Neutron diffraction gives informations also on the *structure* of the adsorbed film, but it cannot tell *where* the condensed phase is placed (for example, capillarity effects, cluster formation due to partial wetting, or bulk condensation in the experimental cell cannot be easily distinguished). The microbalance, on the other hand, cannot distinguish between different film structures: it is always sensitive only to the mass adsorbed onto the substrate. Electron diffraction experiments [low-energy electron diffraction (LEED) and reflection high-energy electron diffraction (RHEED)] are confined to very low fluid density (i.e., to low coverage), while the microbalance works well in a very wide pressure range (up to saturated vapor pressure). It is worth noting that only a graphite fiber microbalance experiment can measure the maximum coverage at saturated vapor pressure.

The device is made of a thin cylindrical graphite fiber (approximately 5 μm in radius and 1 cm in length) that is slightly stretched, and placed into a transverse magnetic field. The fiber is excited into vibration at its resonant frequency ν. Both the frequency and the amplitude of the vibration may be measured through the voltage signal induced by the magnetic field at the fiber ends.

In vacuum the resonant frequency depends on the fiber mass M_w:

$$\nu_0=\sqrt{\tau/4L_w^2M_w}=A\sqrt{1/M_w}, \tag{1}$$

where L_w is the fiber length and τ is the applied tension. When the fiber is surrounded by a fluid, its effective mass becomes

$$M=M_w+M_h+\Delta M, \tag{2}$$

where M_h and ΔM are the hydrodynamic mass (due to the displaced fluid), and the mass of the fluid film adsorbed onto the fiber, respectively.

A simple equation therefore relates the resonant frequency ν in the fluid, with the resonant frequency under vacuum ν_0:

$$\nu=\nu_0\sqrt{M_w/(M_w+M_h+\Delta M)}, \tag{3}$$

and the adsorbed mass is given by

$$\Delta M=M_w\left(\frac{\nu_0^2}{\nu^2}-1-\frac{M_h}{M_w}\right). \tag{4}$$

In order to calculate ΔM one must evaluate the contribution of the hydrodynamic mass M_h. This term is generally not negligible, and sometimes it may be even greater than ΔM. In pure hydrodynamic regime M_h may be derived from the Stokes theory,[6] but when the fluid density is extremely low (i.e., when the molecule mean free path λ is comparable or greater than the fiber diameter) the Stokes theory cannot be used. In this work we give some semiempirical formulas that are valid in a wide range of situations, and that allow evaluating M_h in a simple way.

The microbalance here described is a modified version of the vibrating wire viscometer previously used by the authors to measure the viscosity close to critical points.[7–10] The main change is made in the mechanism used to excite the vibration. The usual way is to feed into the fiber a weak ac current of constant amplitude and proper frequency. This method has two disadvantages. First it produces an output signal that depends on the fiber ohmic resistance, that is temperature dependent: the resistive signal produced by the driving current must be subtracted from the output signal, by placing the fiber in a bridge circuit that requires to be balanced every time the temperature is changed. Second, the exciting current, by joule heating, keeps the fiber at a temperature that is slightly higher than the environment, thus introducing possible errors in the adsorption measurements. These difficulties are avoided by exciting the vibration through a piezoelectric transducer, mechanically coupled to the fiber.

A second new feature of the present design is a greatly increased frequency stability: to reduce the sensitivity of the applied tension to temperature changes, the fiber is now

 0034-6748/91/112772-06$02.00 © 1991 American Institute of Physics

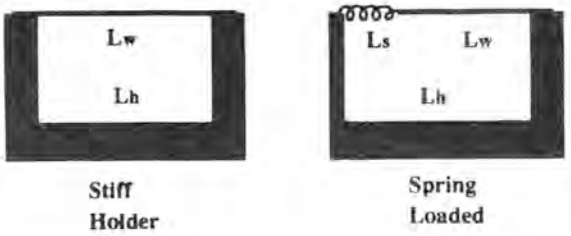

FIG. 1. Simplified model of two stretched-fiber configurations.

stretched by a soft spring, instead of being clamped to a rigid holder. The frequency-lock technique is essentially the same used for the viscometer, with some improvement introduced to reduce the residual phase error, and it is described in detail elsewhere.[11,12]

Here, in Sec. II, we describe the microbalance mechanical setup, and the measuring cell that is designed to reduce the thermal gradients to negligible levels. In Sec. III we present the measuring technique and the calibration procedure. In Sec. IV we report some experimental results of calibrations taken with different fluids and some adsorption measurements of argon on graphite.

II. EXPERIMENTAL APPARATUS

The relative frequency shift due to one atomic layer of argon adsorbed onto the fiber is of the order of 10^{-4}. Therefore, if the microbalance has to resolve a monolayer, the time dependence and the temperature coefficient of the resonant frequency in vacuum must be made appropriately small.

If the fiber ends are clamped to a rigid holder, the difference between the thermal expansion coefficients of the holder and of the fiber produces a strong temperature dependence in the applied tension, and consequently in the resonant frequency: relation (1) gives in fact $\Delta\nu/\nu = \Delta\tau/2\tau$. The resonant frequency stability, both in temperature and in time, may be greatly improved by stretching the fiber through a soft spring.

A sketch of the two different setups is given in Fig. 1. The holder elongation δL_h under the applied tension is assumed to be negligible. In the case of *stiff holder* the tension may be written, in terms of the fiber elastic constant K_w and elongation δL_w, as $\tau = K_w\,\delta L_w$. Assuming a temperature independent K_w, a mismatch between the expansion coefficients of the holder (α_h) and of the fiber (α_w) yields, for a temperature change ΔT, the relative tension change:

$$\frac{\Delta\tau}{\tau}=\frac{\Delta\delta L_w}{\delta L_w}=\frac{(\alpha_h L_h-\alpha_w L_w)\Delta T}{\delta L_w}\approx\frac{(\alpha_h-\alpha_w)L_h}{\delta L_w}\Delta T, \tag{5}$$

where L_h and L_w are the lengths of the holder and of the fiber.

In the case of *spring coupling* the tension is $\tau = K_w\delta L_w = K_s\delta L_s$, where K_s and δL_s are the elastic constant and elongation of the spring. The relative tension change becomes

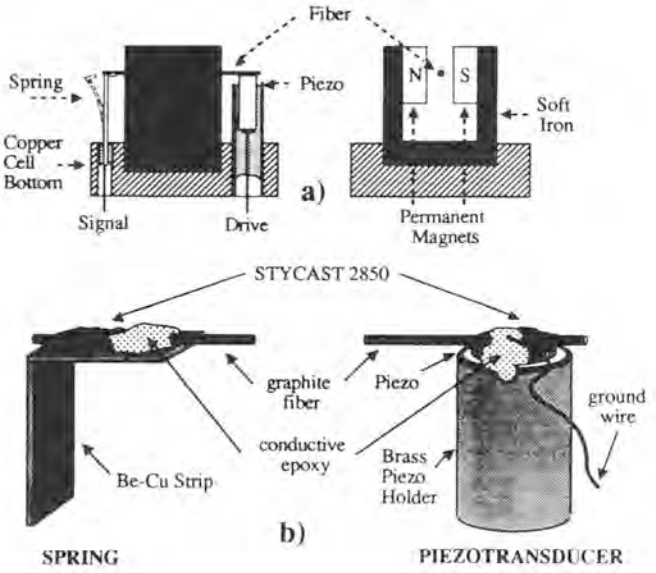

FIG. 2. (a) Scheme of the microbalance setup. (b) Details (drawn not to scale) of the epoxy clamping at the fiber ends.

$$\frac{\Delta\tau^*}{\tau}=\frac{\Delta\delta L_s}{\delta L_s}\approx\frac{K_s}{K_w}\frac{(\alpha_h-\alpha_w)L_h}{\delta L_w}\Delta T. \tag{6}$$

Using a soft spring ($K_s \ll K_w$),[13] the temperature dependence of the resonant frequency is greatly reduced with respect to a stiff holder setup: $\Delta\tau^*/\Delta\tau = \delta L_w/\delta L_s = K_s/K_w \ll 1$. To give an order of magnitude, with $L \approx 1$ cm, $\delta L_s \approx 0.2$ cm, $\alpha_h - \alpha_w \sim 2\times 10^{-5}\,\mathrm{K}^{-1}$ (copper holder), we expect $\Delta\tau^*/\tau\Delta T \approx 10^{-4}\,\mathrm{K}^{-1}$.

Moreover, if we also account for the negative temperature coefficient of the spring elastic constant ($\Delta K_s/K_s = -\beta_s\Delta T$), the effective temperature coefficient of the resonant frequency is further reduced:[14]

$$\frac{\Delta\tau^*}{\tau\Delta T}=\frac{1}{\Delta T}\left(\frac{\Delta\delta L_s}{\delta L_s}+\frac{\Delta K_s}{K_s}\right)\approx\frac{K_s}{K_w}\frac{(\alpha_h-\alpha_w)L_h}{\delta L_w}-\beta_s. \tag{7}$$

Changes in the fiber stiffness, due either to adsorbed *solid* layers or to changes in the Young modulus of the graphite fiber with temperature, have negligible effects on the resonant frequency of the stretched fiber.[15]

The fiber (see Fig. 2) is attached to the piezoelectric transducer[16] and to the spring[17] by means of a strong epoxy resin.[18] The large specific stress applied to the small bonding area leads to a progressive fiber slippage that would be converted, with a rigid holder, into a tension decreasing with time. Applying the tension through a spring does reduce also this effect of a factor K_s/K_w: this may be easily deduced from relation (6) when considering that a slippage Δx corresponds to an effective change of the holder length $\Delta L_h = \Delta x$.

The spring also helps to limit the maximum stress applied to the fiber. This is important when performing thermal cycles between room temperature and the working low temperature, or when baking the fiber to clean the adsorbing surface.[19] Electric contacts are obtained using a con-

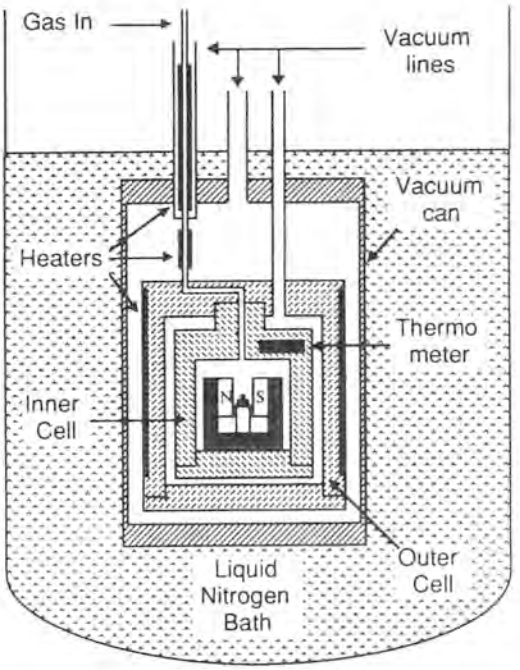

FIG. 3. Schematic of the experimental cell.

ductive epoxy.[20] The output signal electrode is provided by the spring itself. The opposite end of the fiber and the piezoceramic top are grounded. The ground electrode may be electrically insulated from the cell case, to reduce synchronous pickup. The magnetic field is provided by two neodymium-iron-boron permanent magnets[21]: in the gap of 1.5 mm the measured field intensity is ≈ 0.8 T.

The measuring cell, in which the microbalance is placed, is designed to minimize thermal gradients in the fluid. This feature is extremely important when measuring thick film adsorption, because the saturated vapor pressure is determined by the coldest point in the cell. The cell geometry is drawn in Fig. 3. Two concentric thick-wall copper cells are connected by a small cross-section thermal link, and placed inside a vacuum can. The thermoregulating heater is wound around the outer cell, and the inner cell temperature is monitored by a platinum thermometer. In equilibrium conditions a negligible power is exchanged, by radiation, between the two cell walls.

A conservative evaluation of the maximum thermal gradient in the experimental space may be obtained by assuming that the whole heating power is injected at the top of the outer cell, and irradiated from the cell bottom to the vacuum can. With ~ 2.5 mm wall thickness, ~ 50 mm length, and ~ 40 mm mean cell diameter, the negative temperature offset of the cell bottom with respect to the top, is of the order of 0.2 K/W. The top of the inner cell is thermally anchored (by a soldered joint) to the top of the external cell, whereas its bottom is radiatively coupled to the outer cell. Typical values of the power supplied to the heater are much less than 1 W, which gives a maximum temperature difference between any two point in the inner cell smaller than 10^{-6} K. The sample volume is thermoregulated at the working temperature within 0.1 mK. Temperatures much higher than 77 K are obtained by lowering the LN_2 level below the cell bottom, and below 77 K the cryogenic bath is pumped by a mechanical pump. The pressure in the cell is measured by a twin-head capacitive manometer with a maximum resolution of 10^{-3} Torr, and a maximum range of 1000 Torr.[22]

III. CALIBRATION PROCEDURE AND MEASURING TECHNIQUE

When the fiber, of circular cross section and radius r, vibrates in a viscous incompressible fluid, the force per unit length is given in the hydrodynamic regime by the Stokes theory[6]:

$$f = -\pi\rho r^2\left(2\pi\nu K'\frac{\partial y}{\partial t} + K\frac{\partial^2 y}{\partial t^2}\right), \tag{8}$$

where y is the fiber displacement from the rest position, and ρ is the fluid density. K and K' are universal functions of the parameter m:

$$m = (r/2)\sqrt{2\pi\nu\rho/\eta}, \tag{9}$$

where η is the fluid viscosity. An expression of K and K' that may be useful for numerical computation is given in the Appendix.

The hydrodynamic mass M_h is given by

$$M_h = \pi\rho r^2 L_w K. \tag{10}$$

Therefore, by measuring the frequency ν, one calculates the parameter m through relation (9), and relation (10) yields M_h from the known value of the function $K(m)$.

Relation (4) eventually gives the adsorbed mass ΔM as

$$\Delta M = M_w\left(\frac{\nu_0^2}{\nu^2} - 1 - \frac{\rho}{\rho_w}K\right) = \pi\rho_w r^2 L_w\left(\frac{\nu_0^2}{\nu^2} - 1 - \frac{\rho}{\rho_w}K\right), \tag{11}$$

where ρ_w is the fiber density. The adsorbed mass, therefore, may be calculated from the measured frequency shift under two assumptions: first the regime must be hydrodynamic, second the fiber radius and density must be known.

As these assumptions are not generally valid (at low fluid density the system enters a semiballistic regime where the molecule mean free path λ is comparable to the fiber radius, and fibers of the same kind have different density and radius), the microbalance must be calibrated. A calibration may be easily performed using a gas of known viscosity, at a temperature where no adsorption occurs, and at a density where hydrodynamic regime holds.

In these conditions it may be shown[10] that the Stokes functions K and K' satisfy the relations:

$$K = \frac{\rho_w}{\rho}\left(\frac{\nu_0^2}{\nu^2} - 1\right), \tag{12}$$

$$K' = \frac{\rho_w}{\rho\nu}\left(\frac{\nu_0^2}{\nu^2}\Delta\nu - \Delta\nu_0\right), \tag{13}$$

where $\Delta\nu$ and $\Delta\nu_0$ are the resonance width in presence of fluid and in vacuum, respectively. In the full viscous re-

gime relations (12) and (13) are used to calculate K and K', without knowing the value of ρ_w. Because the ratio $K/K'=\mathscr{R}(m)$ does not depend on ρ_w, and it is a monotone function of m, the function $\mathscr{R}(m)$ may be measured and inverted giving:

$$m=m(K/K') \tag{14}$$

$$K=K(\mathscr{R}) \tag{15}$$

$$K'=K'(\mathscr{R}). \tag{16}$$

From (14) and (9) one calculates the radius r, and from (15) and (12), or from (16) and (13), one gets the density ρ_w.

Once the fiber radius and density are known, the gas density may be reduced to values at which the mean free path becomes comparable to (or greater than) the fiber radius, thus departing from the hydrodynamic regime.

With the known r value we may now calculate, for each density, the values of m using relation (9), and the values of $K(m)$ using the relations given in the Appendix. In the semiballistic regime $K(m)$ differs from the measured quantity:

$$F=\frac{\rho_w}{\rho}\left(\frac{\nu_0^2}{\nu^2}-1\right). \tag{17}$$

In order to calculate, from relation (11), the correct value for ΔM also in semiballistic regime, the function K must be replaced by the function F: the goal is therefore to find empirically an analytical expression for F. As it will be shown later, F may be directly obtained from K by an adjusting factor. This approach results much more simply than the complex slip theory used by other authors[23] to correct the Stokes equations in the semiballistic regime.

IV. EXPERIMENTAL RESULTS

The resonant frequency under vacuum ν_0 has values ranging from 10 to 20 kHz, depending on the applied tension ($\tau\simeq 0.5$–2 g), with a stability, at constant temperature, of a few p.p.m. over a period of several days, and a negative temperature coefficient ranging from 10 to 100 ppm/K.

The microbalance has been calibrated at 30 °C by using three gases: He, Ar, and Kr. The measured frequency shift is reported in Fig. 4 as a function of pressure: the resonant frequency under vacuum is $\nu_0\simeq 19$ kHz. The quality factor $Q=\nu/\Delta\nu$ under vacuum is of the order of 10^4 at room temperature, increasing to 10^5 at low temperature. When the fiber is surrounded by gas the quality factor deceases dramatically to values of about 10^2. In this situation, the phase error becomes important, and it is necessary to use the method of the double-phase-locked loop[11,12] to keep a high resolution in the measurement of the resonant frequency.

Here the frequency shift is essentially due to the hydrodynamic mass. Moreover a careful analysis of the data taken at pressures below 1–2 torr, shows that even at room temperature one monolayer is adsorbed onto the fiber, for all the investigated gases. For this reason all the calibration

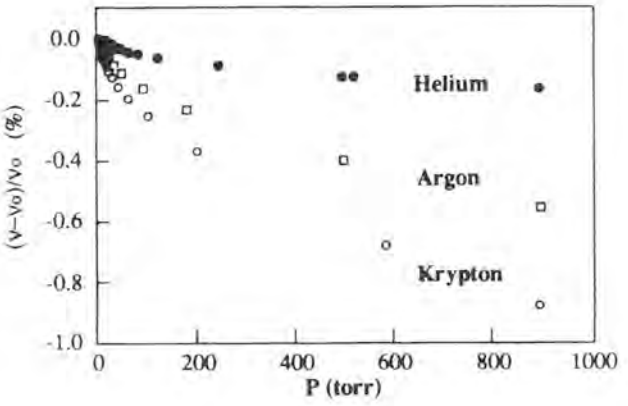

FIG. 4. The fiber resonant frequency measured at room temperature as a function of pressure.

measurements are taken at pressures >3 Torr. To account for the first monolayer, the resonant frequency ν_0, appearing in relation (17), is decreased by an amount corresponding to one layer.

In Fig. 5 we report the values of the ratio F/K as a function of the molecular mean free path λ for the different gases, where the function F is the measured quantity defined by relation (17), K is the Stokes function, and λ is calculated (in c.g.s. units) from the relation[24]:

$$\lambda=\eta/0.499\rho\bar{v}, \tag{18}$$

where $\bar{v}$ is the molecular mean square velocity given by

$$\bar{v}=\sqrt{8RT/\pi M_m}, \tag{19}$$

where T is the absolute temperature, R the universal gas constant, and M_m the molecular mass of the fluid.

A simple analytical form for the function $F(\lambda)$ may be easily obtained by fitting the F/K data of Fig. 5 with an exponential curve:

$$F=K\exp(-\lambda/\alpha). \tag{20}$$

In the range of λ investigated ($\lambda\leqslant 1.2\ \mu$m), the parameter α results to be dependent on the fiber radius and on the molecular mass of the gas:

$$\alpha=0.8r+4.4\times 10^{-4}(1-0.073\sqrt{M_m})\ \text{(c.g.s.)}. \tag{21}$$

Our calibration procedure gives for various fibers $r=(4.5$–$7.5)\ \mu$m and $\rho_w=(1.2$–$2.2)$ g/cm^3, values quite different from the nominal values $r=5\ \mu$m and $\rho_w=2.18$ g/cm^3.

When the measurements cannot be taken fully within the hydrodynamic regime, it may be difficult to calculate the fiber radius and density as explained in Sec. III. In this case the calibration may be performed more simply by minimizing, with respect to r and ρ_w, the sum:

$$\sum_{i=1}^{N}\left(\frac{\nu_0^2}{\nu_i^2}-1-\frac{\rho}{\rho_w}F_i\right)^2, \tag{22}$$

where the index i is extended to all the N experimental measurements taken without adsorption ($\Delta M=0$). The free parameter r appears implicitly in (22) through the F_i.

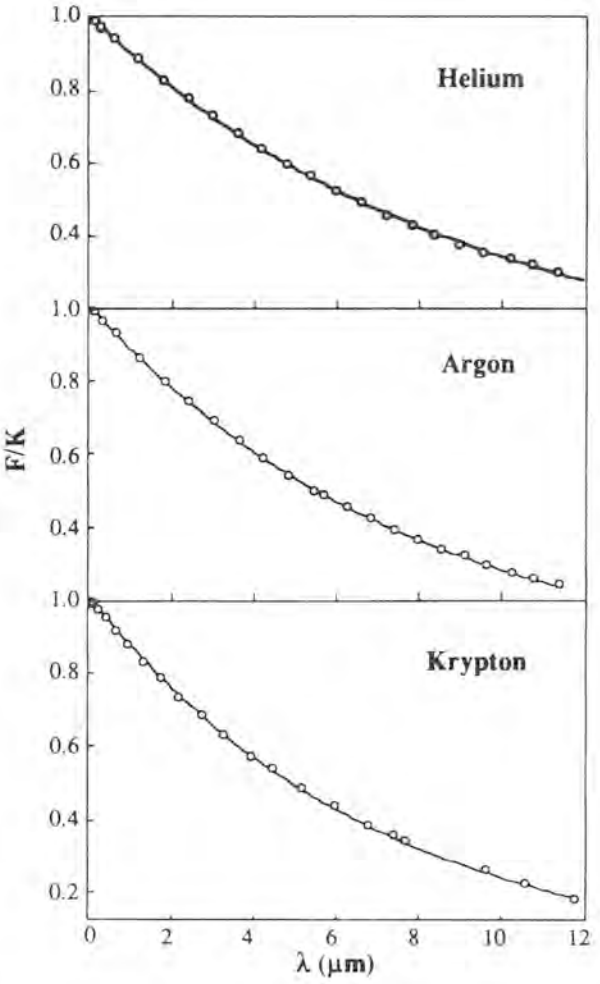

FIG. 5. The ratio F/K calculated as explained in the text vs the molecular mean free path λ at room temperature (open dots). The fitting line is the exponential function given in Eqs. (20) and (21).

The values for r and ρ_w are in agreement (within 3%) with those obtained by the first method. The calibration has been tested also at intermediate temperatures, still above but closer to the critical temperature, where the gas density increases. An example is shown for argon at 167 K in Fig. 6: here the $(M_h + \Delta M)/M_w$ values calculated from the total frequency shift (crosses), are converted into effective mass loading $\Delta M/M_w$ (open dots) by using the empirical function F given in (20) and (21). Clearly $\Delta M/M_w \simeq 0$.

An example of adsorption isotherm taken in argon at $T=66.9$ K, with a PX7 fiber,[25] is reported in Fig. 7. Both the total relative mass change $(M_h + \Delta M)/M_w$, and the actual relative mass change due to the adsorbed film $\Delta M/M_w$ are plotted versus the measured reduced pressure P/P_0 (P_0 is the saturated vapor pressure). At this temperature (below the roughening temperature for Ar on graphite) the change in chemical potential $[\Delta\mu = K_B T \ln(P/P_0)]$ at each layer completion is clearly visible, and the coverage versus pressure curve assumes a stepwise behavior.

The height of the first three adsorption steps is in

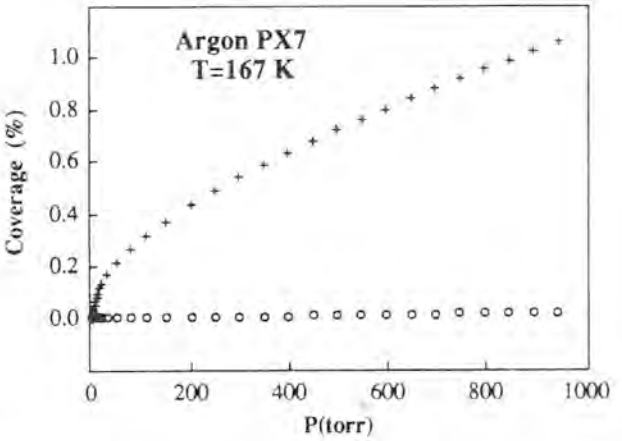

FIG. 6. A test of the calibration performed in argon at 167 K. Crosses: the equivalent coverage due to hydrodynamic mass. Open dots: the actual coverage.

agreement with that predicted for the used PX7 fiber:

$$\left(\frac{\Delta M}{M_w}\right)_{\text{one layer}} = \frac{2\pi r d \rho_a}{\pi r^2 \rho_w} \simeq 10^{-4}, \tag{23}$$

where d ($\simeq 3\times 10^{-8}$ cm) is the monolayer thickness, and ρ_a ($\simeq 1.7$ g/cm^3) is the density of the adsorbate phase. The radius and density of this fiber, as calculated from the calibration at room temperature are $r=5.82$ μm and $\rho_w = 1.36$ g/cm^3, respectively. Also the pressures corresponding to each step (i.e., the chemical potential at layer completion) are in agreement with the values measured by ellipsometric technique[26] and volumetric adsorption isotherms[27] in exfoliated graphite.

The film thickness can be measured up to the saturated vapor pressure P_0, as shown in Fig. 7, and it is limited to a maximum of ~ 6 layers at $T=66.9$ K. The ability of measuring, in a broad range of temperatures, the maximum coverage (i.e.,[28] the film thickness at phase coexistence, above and below the triple point temperature) is one of the most interesting features of the microbalance technique,

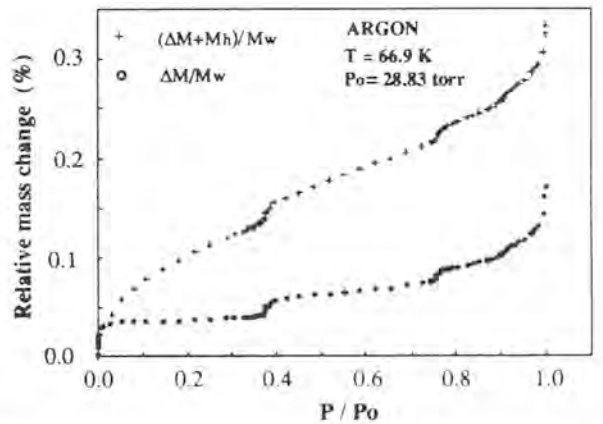

FIG. 7. Adsorption isotherm of argon on a PX7 fiber. Crosses: the total relative mass change $(M_h + \Delta M)/M_w$. Open dots: relative mass change $\Delta M/M_w$ due only to the adsorbed film. P_0 is the saturated vapor pressure.

and it has been used to prove a triple point wetting behavior for argon[3] and other noble gases on graphite.

ACKNOWLEDGMENTS

The authors would like to thank Giorgio Delfitto for his valuable help on assembling and testing the experimental apparatus, and Attilio Donà for his active collaboration in data handling and reduction. The present work was supported by Consorzio Interuniversitario Struttura della Materia and Consiglio Nazionale delle Ricerche, Rome, Italy.

APPENDIX

The Stokes functions K and K', for $m<1$, are defined by the following formula (No. 105 in the original article):[6]

$$K+jK'=1+\frac{2}{m^2}\,\frac{-LM_o+(\pi/4)M_e-(1/2)M'_o+N_o+j[(\pi/4)M_o+LM_e-(1/2)(1-M'_e)-N_e]}{-(\pi/4)M'_o+L(1-M'_e)+N'_e+j[-LM'_o-(\pi/4)(1-M'_e)+N'_o]},$$

where $j=\sqrt{-1}$ is the imaginary unit, $L=\ln(m)+\Lambda$, ($\Lambda=0.57721566...$ is the Euler constant), and M_o, M'_o, M_e, M'_e, N_o, N'_o, N_e, and N'_e are functions of m that may be written in a form appropriated for numerical computation as follows:

$$M_o=\sum_{i=0}^{\infty}\left[(-1^i)\,\frac{m^{2(2i+1)}}{(2i+1)!2i!}\right]=\sum_{i=0}^{\infty}a_i,$$

$$M'_o=\sum_{i=0}^{\infty}\left[\frac{a_i}{(2i+1)}\right],$$

$$M_e=\sum_{i=0}^{\infty}\left[\frac{m^2a_i}{(2i+1)(2i+2)}\right]=\sum_{i=0}^{\infty}b_i,$$

$$M'_e=\sum_{i=0}^{\infty}\left[\frac{b_i}{(2i+2)}\right],$$

$$N_o=\sum_{i=0}^{\infty}\left[a_i\sum_{n=1}^{2i+1}\frac{1}{n}\right]=\sum_{i=0}^{\infty}[a_iS_{2i+1}],$$

$$N'_o=\sum_{i=0}^{\infty}\left[\frac{a_iS_{2i+1}}{(2i+1)}\right],$$

$$N_e=\sum_{i=0}^{\infty}[b_iS_{2i+2}],$$

$$N'_e=\sum_{i=0}^{\infty}\left[\frac{b_iS_{2i+2}}{(2i+2)}\right].$$

In our experimental situation a very good approximation is obtained by truncating the series at $i=10$.

[1] C. Bartosh and S. Gregory, Phys. Rev. Lett. **54**, 2513 (1985).
[2] P. Taborek and L. Senator, Phys. Rev. Lett. **57**, 218 (1986).
[3] L. Bruschi, G. Torzo, and M. W. H. Chan, Europhys. Lett. **6**, 541 (1988).
[4] G. Zimmerli and M. W. Chan, Phys. Rev. B **38**, 8760 (1988).
[5] A recent review of adsorption studies with these techniques may be found in H. Taub, G. Torzo, H. J. Lauter, and S. C. Fain Jr., eds., *Phase Transitions in Surface Films* 2, NATO ASI Series, (Plenum, New York, 1991).
[6] G. Stokes, *Mathematical and Physical Papers* (Cambridge University, London, 1922), Vol. III.
[7] L. Bruschi and M. Santini, Rev. Sci. Instrum. **46**, 1560 (1975).
[8] L. Bruschi, G. Mazzi, M. Santini, and G. Torzo, J. Low Temp. Phys. **29**, 63 (1977).
[9] L. Bruschi and M. Santini, Phys. Lett. A **73**, 395 (1979).
[10] L. Bruschi, Il Nuovo Cimento **1**, 361 (1982).
[11] L. Bruschi and G. Torzo, Rev. Sci. Instrum. **58**, 2181 (1987).
[12] L. Bruschi, R. Storti, and G. Torzo, Rev. Sci. Instrum. **58**, 1960 (1987).
[13] The ratio K_v/K_{ii} may be easily made of the order of 10^{-3}.
[14] In some temperature range, in fact, the temperature coefficient of the resonant frequency does change sign.
[15] An evaluation of the resonant frequency sensitivity to stiffness changes is given by the ratio $\gamma=f_v/f_\tau$ of the stiffness restoring force to the tension restoring force. Letting $f_v=Yr^4(\partial^4y/\partial x^4)$, and $f_\tau=\tau(\partial^2y/\partial x^2)$ [where $Y\simeq10^{11}$Pa is the graphite Young modulus, $(\partial y/\partial x)$ the gradient of the lateral displacement along the fiber axis, and $\tau=4\pi\rho_{ii}v^2l_{ii}^2r^2$], in our setup we get $\gamma\simeq2\times10^{-3}$. Because the relative change in f_v for a film thickness up to 100 atomic layers, is less than 1%, the error introduced by neglecting the solid film stiffness effect in our microbalance experiment is of the order of few ppm.
[16] A cylindrical ceramic (3 mm diameter, 6 mm length) taken from a commercial piezolighter.
[17] A thin Be-Cu strip, (dimensions $\simeq10$ mm$\times1$ mm$\times0.1$ mm).
[18] The epoxy is Stycast 2850FT, with a shear strength of 58×10^6 Pa (from Bulletin 7272A, Emerson & Cumings Europe, Oeven, Belgium). The fiber tensile strength is $\simeq3\times10^9$ Pa. The fiber length covered by the epoxy is about 1 mm (corresponding to an effective glued surface $\simeq3\times10^{-4}$ cm^2), and the resin is baked at 120 °C, while keeping the spring loaded by means of a stop screw that is carefully removed after the epoxy is hardened.
[19] Adsorption experiments require a careful cleaning of the substrate *in situ*, by heating it at high temperature in high vacuum. This may be easily performed in this microbalance by feeding an electric current of few milliampere through the fiber.
[20] Eccobond 66C, with Catalyst 24LV (Emerson & Cumings Europe, Oeven, Belgium).
[21] Type BLNI 619/*p*, Magnet Developments Ltd, Swindon, England.
[22] Model PDR-C-2, MKS Instruments Inc., Burlington, MA.
[23] H. Hojgaard, H. Smith, P. Wolfe, K. Nagai, and T. Maack Bisgaard, J. Low Temp. Phys. **41**, 473 (1980).
[24] J. Kestin and W. Leidenfrost, Physica **25**, 1033 (1959).
[25] P×7 (also named P-130) is a mesophase-pitch-derived graphite fiber produced by Amoco Performance Products Inc., Parma Technical Center, Ohio.
[26] G. B. Hess, in *Phase Transitions in Surface Films* 2, edited by H. Taub, G. Torzo, H. J. Lauter, and S. C. Fain Jr., NATO ASI Series (Plenum, New York, 1991).
[27] F. Ser, Y. Larher, and B. Gilquin, Molec. Phys. **67**, 1077 (1989).